ENGINEERING TRANSACTIONS • *Engng. Trans.* • **48**, 4, 373–393, 2000
Polish Academy of Sciences • Institute of Fundamental Technological Research
10.24423/engtrans.581.2000

STATIC AND STABILITY ANALYSIS OF SHELLS WITH LARGE DISPLACEMENTS AND FINITE ROTATIONS

J. MARCINOWSKI

WROCŁAW UNIVERSITY OF TECHNOLOGY
Wybrzeże Wyspiańskiego 27, 50–370 Wrocław, Poland

The paper deals with large displacements and finite rotations of elastic shells subjected to the action of external loads. The numerical approach to the problem based on the finite element method in displacement formulation is presented. The degenerated finite element originally introduced by AHMAD *et al.* [1] and subsequently supplemented by MARCINOWSKI [2] was used in this paper. This very element was essentially suitable for shell problems exhibiting small and moderate rotations, but there exists a possibility to apply it also to problems with finite rotations, provided the updated Lagrangian formulation is adopted. Details of such an approach were presented in the paper. Several examples taken from the literature and confirming the correctness of the applied approach were included.

1. INTRODUCTION

There are many problems in which the shell analysis must be conducted within the range of large displacements and finite rotations. Postbuckling analysis of shells and plates are examples of such problems.

Large rotations frequently encountered in nonlinear analysis of shells can be accounted for on the level of the adopted shell theory (cf. e.g. GRUTTMANN *et al.* [3], BUECHTER and RAMM [4], CHRÓŚCIELEWSKI [5], SANSOUR and BUFLER [6]), or on the level of the shell element formulation, which takes into account finite rotations (cf. e.g. SURANA [7]). This second approach will be adopted generally in this paper.

The finite element originally introduced by AHMAD *et al.* [1] and then supplemented by PAWSEY and CLOUGH [8] and ZIENKIEWICZ *et al.* [9], and after that adjusted to nonlinear problems by MARCINOWSKI [2], was adopted in this work. Due to linearisation of the displacement field with respect to the nodal

rotational parameters, the element can be adopted only to geometrically nonlinear problems with moderate rotations. In spite of this obvious drawback, there is a possibility of applying it to problems with rotations of arbitrary magnitude. The main idea of the presented approach consisits in successive changing of the reference configurations performed in the course of nonlinear analysis. This approach is well known in mechanics of solids and is called the updated Lagrangian formulation (cf. BATHE *et al.* [10], STRICKLIN and HAISLER [11]). The point is that the whole analysis is divided into stages symbolically shown in Fig. 1. The procedure begins with the initial undeformed configuration (Conf. 1 in Fig. 1) and is continued till the largest registered nodal rotation assumes the limit value given in advance (e.g. 0.05 rad). It is the signal for changing the reference configuration from Conf. 1 to Conf. 2, shown symbolically in Fig. 1. Further deformations of the shell are being described with respect to the configuration Conf. 2 which is neither undeformed nor free of stresses. Of course, both these factors must be taken into account in the governing equations which describe this stage of analysis.

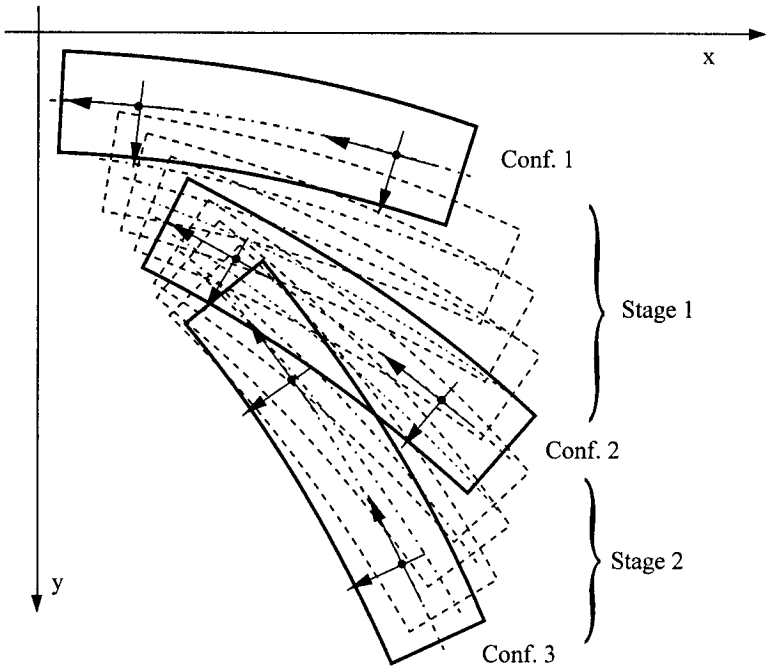

FIG. 1. Successive changing of reference configurations.

This approach guarantees that the displacement approximation applied in the finite element will be always correct and arbitrarily large rotations will be accounted for in a proper way.

2. Governing equations

The general principle of mechanics of solids, the principle of virtual displacements (cf. MALVERN [12]), will be the foundation on which the whole calculation model will be constructed. This principle written for any reference configuration takes the following form:

$$\int_V S_{IJ}\delta E_{IJ}dV - \int_V f_{oI}\delta u_I dV - \int_S t_I^o \delta u_I dS = 0, \tag{2.1}$$

where V and S denote the whole volume and the whole external surface of the body in the current configuration which is not free of stresses and strains. S_{IJ} are components of the second Piola-Kirchhoff stress tensor in the analysed configuration, and δE_{IJ} are the variations of components of the Green-Saint-Venant strain tensor produced by virtual displacements δu_I. f_{oI} and t_I^o are the body forces and surface tractions (external loads) acting on the body.

Two last terms in Eq. (2.1) express the virtual work done by external (body and surface) forces and because only conservative loadings are taken into account, they are calculated in the first stage of analysis when the reference configuration coincides with the initial unstrained and stress-free configuration.

The principle of virtual displacements can be written in a discrete form by means of the finite element method in displacement formulation (cf. MARCINOWSKI [2]). For this very element it is possible to write the components of strains and stresses in the following form (cf. MARCINOWSKI [2]):

$$\varepsilon^k = (B_i^k + W_{ij}^k d_j)d_i + \varepsilon_o^k, \tag{2.2}$$

$$\sigma^k = D^{kl}(\varepsilon^l - \varepsilon_o^l) + \sigma_o^k, \tag{2.3}$$

or

$$\sigma^k = D^{kl}(B_i^l + W_{ij}^l d_j)d_i + \sigma_o^k, \tag{2.4}$$

where ε_o^i and σ_o^i are initial strains and initial stresses present in the reference configuration. B_i^k and W_{ij}^k are the quantities with two and three indices (respectively), dependent on the shape functions and the geometry of finite element, and not dependent on the nodal displacements d_i. W_{ij}^k is symmetric with respect to the pair i, j. Only linearly elastic materials are considered and D^{kl} is the matrix of material constants (cf. MARCINOWSKI [2]).

Because nodal displacements d_i are measured with respect to the reference configuration (they are not total displacements), at the beginning of the analysis all $d_i = 0$, so that

$$\varepsilon^i = \varepsilon^i_o, \qquad \sigma^i = \sigma^i_o, \tag{2.5}$$

as follows from Eqs. (2.2) and (2.4).

Let us write the variation of strains using Eq. (2.2).

$$\delta\varepsilon^k = \frac{\partial \varepsilon^k}{\partial d_m}\delta d_m = B^k_m \delta d_m + 2W^k_{ij} d_i \delta d_j = (B^k_m + 2W^k_{ij} d_j)\delta d_i. \tag{2.6}$$

It is seen that the initial strains ε^i_o do not act upon the variations of strains.

Let us assume that the intensity of all forces is defined by the single parameter λ. According to the finite element method (cf. ZIENKIEWCZ [13]), all external forces on the reference level defined by $\lambda \equiv 1$, are replaced by nodal forces F_i calculated only once at the very beginning of the analysis. Therefore, the actual state of loading is determined by products λF_i.

After these modifications, the principle of virtual displacements (2.1) can be expressed as follows:

$$\sum_{(e)} \left(\int_{V^e} \sigma^k \delta\varepsilon^k dv - \lambda F_i \delta d_i \right) = 0, \tag{2.7}$$

where V^e denotes the volume of finite element e in the current configuration, the symbol $\sum_{(e)}$ denotes summation over all finite elements (cf. ZIENKIEWICZ [13]).

Substituting Eqs. (2.4) and (2.6) into (2.7) one obtains

$$\sum_{(e)} \left(\int_{V^e} (B^k_i + 2W^k_{ij} d_j)\delta d_i \left[D^{kl}(B^l_m + W^l_{mn} d_n) d_m + \sigma^k_o \right] dv - \lambda F_i \delta d_i \right) = 0. \tag{2.8}$$

This relationship must be true for all nodal virtual displacements δd_i. Hence

$$\Psi_i(\{d\}, \lambda) = \sum_{(e)} \{K_{im} + [(G_{imn} + C_{inm} + H_{ijmn} d_j) d_n]\, d_m + R^o_i + S^o_{ij} d_j - \lambda F_i\} = 0, \tag{2.9}$$

where

$$K_{im} = \int_{V^e} B^k_i D^{kl} B^l_m dv, \qquad G_{imn} = \int_{V^e} B^k_i D^{kl} W^l_{mn} dv, \tag{2.10}$$

$$C_{inm} = 2\int_{V^e} W^k_{in} D^{kl} B^l_m dv, \qquad H_{ijmn} = 2\int_{V^e} W^k_{ij} D^{kl} W^l_{mn} dv, \tag{2.11}$$

$$R^o_i = \int_{V^e} B^k_i \sigma^k_o dv, \qquad S^o_{ij} = 2\int_{V^e} W^k_{ij} \sigma^k_o dv. \tag{2.12}$$

The relationship (2.9) can be expressed in traditional, matrix notation in the following way:

$$\{\Psi(\{d\},\lambda)\} = [K_N]\{d\} - \lambda\{F\} + \{R\} = \{0\}, \tag{2.13}$$

where the vector $\{R\}$follows from the summation of terms $R_i^o + S_{ij}^o d_j$. This is the nonlinear set of algebraic equations with respect to unknown nodal displacements d_i. The collection of solutions of this set of equations for the chosen range of loading parameter λ creates the curve in the load-displacements hyperspace called the equilibrium path. The nonlinearity of the set (2.13) is embedded in the nonlinear stiffness matrix $[K_N]$ (cf. (2.9)) and it is seen that this is the polynomial relationship.

3. Solution of the nonlinear set of equilibrium equations

To solve the nonlinear set of equilibrium equations, the Newton-Raphson method is applied. To this end let us assume that the approximate solution of the set (2.13) $\{d^e\}$, λ^e is known in advance. The exact solution will be searched in the form

$$\{d\} = \{d^e\} + \Delta\{d\}, \quad \lambda = \lambda^e + \Delta\lambda. \tag{3.1}$$

The value of the vector $\{\Psi(\{d\},\lambda)\}$ at this point will be searched in the form of linear expansion about the point $\{d^e\}$, λ^e:

$$\{\Psi(\{d\},\lambda)\} \cong \{\Psi(\{d^e\},\lambda^o)\} + \left.\frac{\partial\{\Psi\}}{\partial\{d\}}\right|^e \Delta\{d\} + \left.\frac{\partial\{\Psi\}}{\partial\lambda}\right|^e \Delta\lambda = \{0\}, \tag{3.2}$$

or using the index notation

$$\Psi_i(\{d\},\lambda) \cong \Psi_i(\{d^e\},\lambda^e) + \left.\frac{\partial\Psi_i}{\partial d_j}\right|^e \Delta d_j + \left.\frac{\partial\Psi_i}{\partial\lambda}\right|^e \Delta\lambda = 0, \quad i = 1,2,...,N, \tag{3.3}$$

where N is the number of degrees of freedom.

Knowing the explicit form of Ψ_i (cf. (2.9)) one can calculate:

$$\left.\frac{\partial\Psi_i}{\partial d_j}\right|^e \Delta d_j + \left.\frac{\partial\Psi_i}{\partial\lambda}\right|^e \Delta\lambda = \sum_{(e)} \left[(\Omega_{im}^e + S_{im}^o)\Delta d_m - F_i\Delta\lambda\right], \tag{3.4}$$

where

$$\Omega_{im}^e = K_{im} + \left[2G_{imn} + C_{inm} + C_{imn} + (2H_{ijmn} + H_{imjn})d_j^e\right] d_n^o. \tag{3.5}$$

In this manner the i-th linear algebraic equation for the corrections Δd_m, $\Delta\lambda$ sought for, is obtained in the following form:

$$\sum_{(o)} [(\Omega^e_{im} + S^o_{im})\Delta d_m - \Delta\lambda F_i] = -\Psi_i(\{d^e\}, \lambda^e). \tag{3.6}$$

The procedure is of an iterative character. Δd_m, $\Delta\lambda$ obtained from (3.6) are substituted to (3.1) and this result is treated as the approximate solution to the following steps of iterations. Details of the procedure are presented in the paper of MARCINOWSKI [2].

In the set (3.6) only Ψ^e_i is being updated whereas $\Omega^e_{im} + S^o_{im}$ are kept in the form which they have taken at the first iteration step. Such a procedure is characteristic for the modified Newton-Raphson method.

The iteration process is finished when the condition

$$\frac{|\Delta\{d\}, \Delta\lambda|}{|\{d\}, \lambda|} \leq \varepsilon \tag{3.7}$$

is fulfilled. ε is the dimensionless value given in advance. In most cases it was assumed that $\varepsilon = 1 \cdot 10^{-3}$ and only in some particular problems it was reduced to the value $\varepsilon = 1 \cdot 10^{-5}$. Norms present in the formula (3.7) were calculated as follows:

$$|\Delta\{d\}, \Delta\lambda| = \sqrt{\Delta\overline{d}_i \Delta\overline{d}_i + \Delta\lambda^2}, \qquad |\{d\}, \lambda| = \sqrt{\overline{d}_i \overline{d}_i + \lambda^2}. \tag{3.8}$$

As far as the calculation of nonlinear equilibrium paths is concerned, the procedure was exactly the same as the one presented by MARCINOWSKI [2] and by MARCINOWSKI and ANTONIAK [14]. The approximate solution was constructed also as a cubic Taylor expansion about the last known point on the path (cf. MARCINOWSKI [2]).

4. GENERAL STRATEGY OF CALCULATIONS

As mentioned in the Introduction, there is a necessity to apply the updated Lagrangian description. The reference configuration will be updated every time when the maximum nodal rotation exceeds the limiting value given in advance. To ensure that the adopted linear displacement approximation with respect to nodal rotations is true, this limiting value must be smaller than 0.1 rad (5.73°). In this way the maximum error caused by the adopted displacement approximation will never exceed 0.5 %.

The general strategy of the proposed approach will be presented in the form of succeeding operations, which should be executed to ensure that the given problem

dealing with geometrically nonlinear shells with large displacements and finite rotations is solved correctly. For better clarity, the description was illustrated by Fig. 1.

STAGE I – the description of motion with respect to the initial, undeformed and stress-free configuration (Conf.1 in Fig. 1).

• Reading the geometrical and material data.

• The nonlinear analysis controlled by the chosen displacement parameter exactly as in the case of moderate rotations (cf. MARCINOWSKI [2]).

• At the instant when the maximum nodal rotation exceeds the limiting value α_{lim} (e.g. 0.05 rad) given in advance:

– storing of final displacements of the stage I $\{d^I\}$,

– storing of final stresses σ_o^I of this stage at every Gauss point of all elements,

– generation of new nodal coordinates corresponding to final displacements of this stage; it means updating the reference configuration (details below).

STAGE II – the description of motion with respect to the deformed configuration Conf. 2.

• Reading the new geometrical data referring to the new configuration Conf. 2.

• Reading the stresses calculated in the previous stage (details below).

• The nonlinear analysis controlled by the chosen displacement parameter based on the principle of virtual displacements in which initial stresses were taken into account.

• At the instant when the maximum nodal rotation exceeds the limiting value α_{lim} (e.g. 0.05 rad) given in advance:

– generation of global nodal displacements for this stage $\{d^{II}\}$,

– generation of total nodal displacements $\{d^t\} = \{d^I\} + \{d^{II}\}$,

– calculation of final stresses σ_o^C of this stage at every Gauss point of all elements,

– generation of new nodal coordinates corresponding to final displacements of this stage (actualisation of the reference configuration).

STAGE III and succeeding stages – the description of motion with respect to the deformed configuration Conf. 3 and succeeding configurations (respectively):

• Operations similar to those from the Stage II.

It is worthy to discuss in details two of the operations specified above. The first of them is actualisation of geometry on the basis of the calculated nodal displacements.

Let us consider the local coordinate system at the node i of the finite element (cf. Fig. 2). We will find the displacement of the point A as a result of two succeeding rotations of the unit segment $\overline{OA}$. After the rotation by angle α_i around the axis determined by the vector $\mathbf{v}_{2i}$, the point A will take the position A'. Coordinates of this point in the local coordinate system are: $\sin\alpha_i$, 0 $\cos\alpha_i$.

After the succeeding rotation by the angle β_i around the axis determined by the vector $\mathbf{v}_{1i}$ the point A' will take the position A''. Coordinates of this point in the local coordinate system are: $\sin\alpha_i$, $-\cos\alpha_i \sin\beta_i$, $\cos\alpha_i \cos\beta_i$. The vector $\mathbf{F} = \overline{AA''}$ will be equal to

$$\mathbf{F} = \sin\alpha_i \mathbf{v}_{1i} - \cos\alpha_i \sin\beta_i \mathbf{v}_{2i} + (\cos\alpha_i \cos\beta_i - 1)\mathbf{v}_{3i}. \tag{4.1}$$

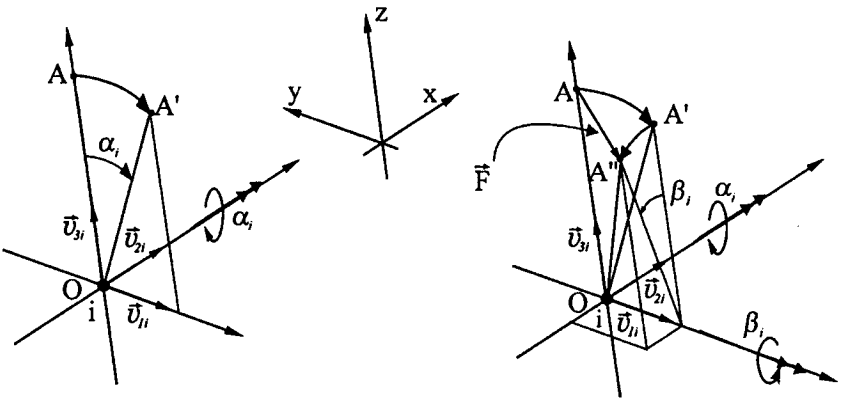

FIG. 2. Rotational transformation.

New coordinates of the top nodes (index t) and the bottom nodes (index b) corresponding to the node i of arbitrary element are calculated as follows:

$$\begin{aligned}
\text{new}\begin{Bmatrix} x \\ y \\ z \end{Bmatrix}^t_i &= \text{old}\begin{Bmatrix} x \\ y \\ z \end{Bmatrix}^t_i + \begin{Bmatrix} u \\ v \\ w \end{Bmatrix}^m_i + \frac{t_i}{2}\begin{Bmatrix} F_{ix} \\ F_{iy} \\ F_{iz} \end{Bmatrix}, \\
\text{new}\begin{Bmatrix} x \\ y \\ z \end{Bmatrix}^b_i &= \text{old}\begin{Bmatrix} x \\ y \\ z \end{Bmatrix}^b_i + \begin{Bmatrix} u \\ v \\ w \end{Bmatrix}^m_i - \frac{t_i}{2}\begin{Bmatrix} F_{ix} \\ F_{iy} \\ F_{iz} \end{Bmatrix},
\end{aligned} \tag{4.2}$$

where u, v, w are components of displacements of the middle node (index m) in the global coordinate system and t_i is the thickness of the shell at the node i.

It is worthy to mention that the above formula corresponds to the exact rotational transformation relationship when two succeeding rotations are superimposed. Taking these formulae in their exact form is very important from the point of view of the precision of further solutions.

The other step of the presented procedure deserving a detailed discussion is the calculation of stresses at the beginning of the new configuration using the stresses known from the last step of the previous configuration.

Let us focus our attention on any configuration. Let it be the configuration Conf. i in Fig. 3. Stresses are calculated in consecutive cycles of the current stage in the reference configuration because they are the second Piola-Kirchhoff stresses. They are measured with respect to the surface of the reference configuration in the local coordinate system x_i^o of this very configuration. At the instant of changing of the reference configuration from Conf. i to Conf. $i+1$, there is need to write the stresses calculated at the last cycle of the stage in the new local coordinate system x_i^t (cf. Fig. 3) of the configuration Conf. $i+1$. As a matter of fact, this new coordinate directions are just convections of material coordinates (cf. ODEN [15], KLEIBER [16]) from the configuration Conf. i. One can prove that there exists the following relationship (cf. KLEIBER [16])

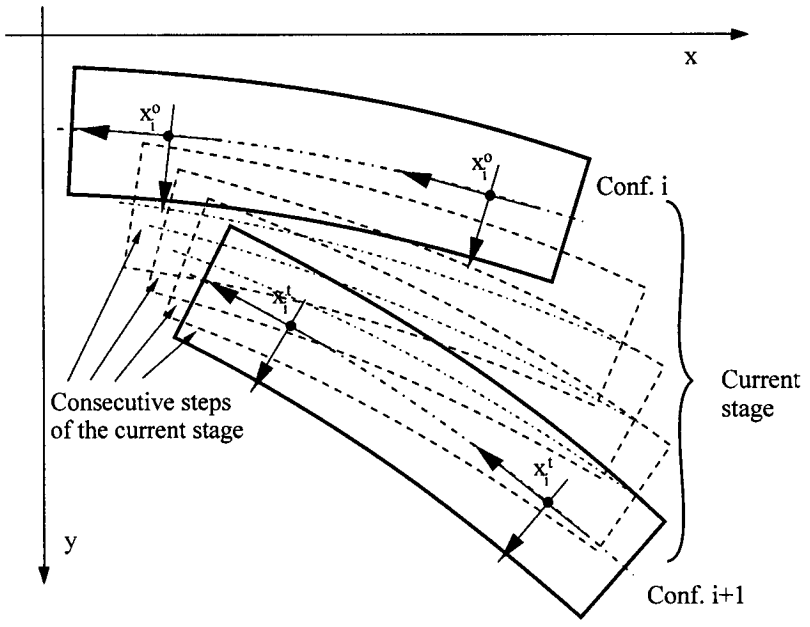

FIG. 3. Stresses in convected coordinates.

$$\hat{S}_{KL} \equiv \frac{1}{J} S_{KL}, \tag{4.3}$$

where $\hat{S}_{KL}$ are components of stresses in the current configuration Conf. $i+1$ in the convected coordinate system x_i^t, and S_{KL} are their counterparts in the configuration Conf. i in the coordinate system x_i^o. Both stresses are the second Piola-Kirchhoff stresses. $J = \det\left[\dfrac{\partial x_i}{\partial X_J}\right]$ is the determinant of the deformation gradient (cf. MALVERN [12]). Stresses $\hat{S}_{KL}$ are the initial stresses (denoted by σ_o^i

in Eq. (2.3) and in the subsequent formulae) needed in succeeding cycles of the analysis in the whole next stage.

The determinant J can be easily calculated at every Gauss point from the formula (cf. MALVERN [12]):

$$J = \frac{dv}{dV} \cong 1 + \varepsilon_x + \varepsilon_y + \varepsilon_z, \tag{4.4}$$

where dv and dV are infinitesimal volumes in configurations Conf. $i+1$ and Conf. i (respectively), ε_x, ε_y, ε_z are strains in directions x, y, z registered in the current stage.

In the local coordinate system adopted here (cf. MARCINOWSKI [2]) $\varepsilon_z = 0$, and therefore

$$J \cong 1 + \varepsilon_x + \varepsilon_y. \tag{4.5}$$

The sequence of operations described above was implemented in the computer program applied then to the solution of many problems. Some examples confirming the correctness of the adopted approach are presented below.

5. ILLUSTRATIVE EXAMPLES

5.1. Cantilever bent by the moment

There exists an analytical solution of the beam shown in Fig. 4. This is the reason why this very problem is very often taken as the method of verification of procedures in which large rotations were taken into account.

According to the Euler-Bernoulli theory of bending, there exists linear relationship between the bending moment M and the angle φ. This relationship takes the form

$$M = \frac{EI}{L}\varphi, \tag{5.1}$$

where L is the length of cantilever, E is Young's modulus, $I = \dfrac{bh^3}{12}$ is the moment of inertia of the beam cross-section.

Let us introduce the dimensionless angle parameter η defined as follows:

$$\eta = \frac{\varphi}{2\pi} = \frac{ML}{2\pi EI}, \tag{5.2}$$

and dimensionless displacements of the cantilever tip (cf. Fig. 4)

$$(5.3) \qquad \overline{u}_k = \frac{u_k}{L} = 1 - \frac{\sin\varphi}{\varphi} = 1 - \frac{\sin 2\pi\eta}{2\pi\eta}, \qquad \overline{w}_k = \frac{w_k}{L} = \frac{1}{\varphi}(1 - \cos\varphi)$$

$$= \frac{1}{2\pi\eta}(1 - \cos 2\pi\eta),$$

where $M \in \langle\, 0, \dfrac{2\pi EI}{L} \,\rangle$, and $\eta \in \langle 0, 1 \rangle$.

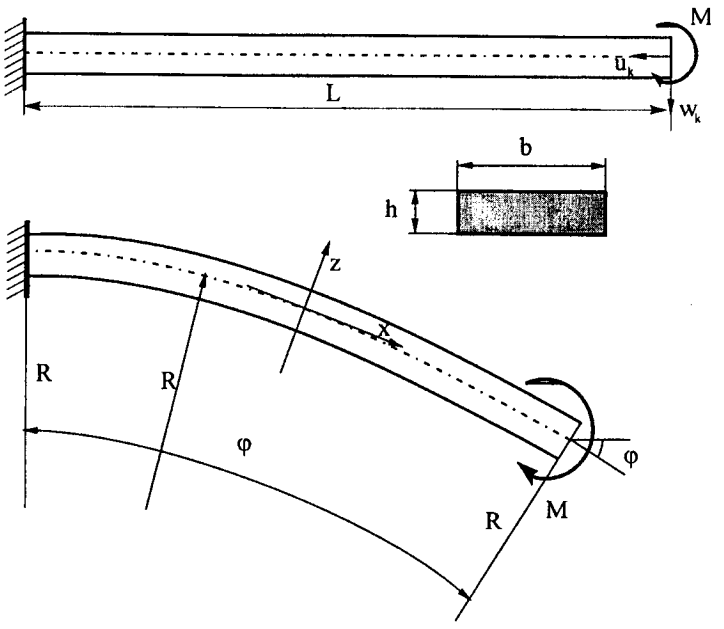

FIG. 4. The cantilever bent by a moment.

Geometrical and material data adopted in the numerical analysis are shown in Fig. 5. The discrete model of the plate strip was obtained as a result of division of the strip into five 8-node (40 degrees of freedom (d.o.f.)) elements. As a result, the discrete model of 140 d.o.f. was obtained. The reference configurations were changed when maximum rotations have reached 0.05 rad (in the initial stage of analysis) or 0.02 rad (in the final stage of analysis). Results of the numerical analysis of this problem are shown in Fig. 5 by markers. The analytical solution is shown by solid lines. Characteristic configurations corresponding to angles $\varphi = \dfrac{\pi}{2}, \pi, \dfrac{3}{2}\pi$ and 2π are shown in the figure as well. The quite good agreement between the numerical and analytical solutions is seen in the figure.

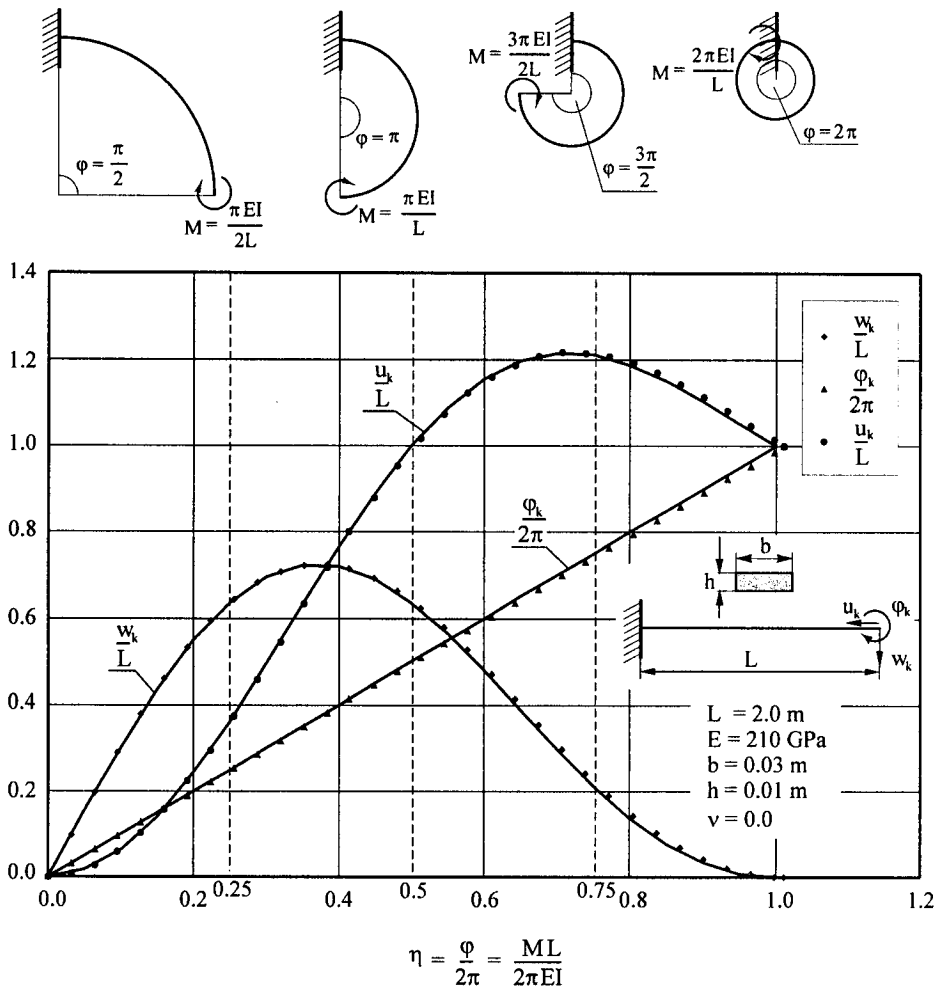

FIG. 5. Bending of a cantilever. Numerical and analytical solutions.

5.2. Cantilever bent by the concentrated force

This is the other problem, which can be used for verification of the numerical program. The analytical solution of the problem was presented by FRISCH-FAY [17]. Knowing all geometrical and material parameters shown in Fig. 6, one can calculate coordinates of the current point C of the cantilever from the formulae

$$x = \frac{L}{\sqrt{c}}\{\cos\alpha[2E(p,n) - 2E(p,m) - F(p,n) + F(p,m)] + 2p \cdot \sin\alpha \cdot (\cos m - \cos n)\}, \tag{5.4}$$

$$y = \frac{L}{\sqrt{c}}\{2p\cos\alpha(\cos m - \cos n) + \sin\alpha[F(p,n) - F(p,m) - 2E(p,n) + 2E(p,m)]\}, \tag{5.5}$$

where:

$$p = \sin\frac{\alpha+\gamma}{2}, \qquad m = \arcsin\frac{\sin\frac{\alpha}{2}}{p}, \qquad n = \arcsin\frac{\sin\frac{\alpha+\varphi}{2}}{p}, \tag{5.6}$$

$$c = \frac{L^2P}{EI}.$$

γ is the angle of rotation of the free end of the cantilever and φ is the angle of rotation of the current point of the rod axis (cf. Fig. 6). $F(p,n)$ and $E(p,n)$ are elliptic functions of the first and second kind (respectively):

$$F(p,n) = \int_0^n \frac{d\psi}{\sqrt{1-p^2\sin^2\psi}}, \qquad E(p,n) = \int_0^n \sqrt{1-p^2\sin^2\psi}\,d\psi. \tag{5.7}$$

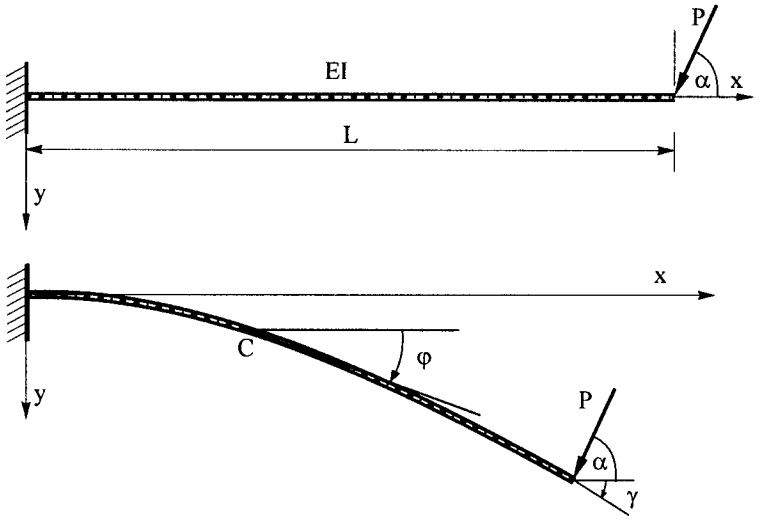

FIG. 6. The cantilever bent by a concentrated force.

To calculate coordinates x, y of an arbitrary point of the rod axis, the angle γ is assumed first and then the corresponding force P is calculated from the formula:

$$P = \frac{EI}{L^2}[K(p) - F(p,m)]^2, \tag{5.8}$$

where $K(p) = \int_0^{\pi/2} \frac{d\psi}{\sqrt{1 - p^2 \sin^2 \psi}}$ is the elliptic integral of the first kind (absolute), and parameters p and m are obtained from formulae (5.6). Taking then the whole series of angles φ from the interval $\langle 0, \gamma \rangle$ and calculating the coefficient c from the formula (5.6), both coordinates x, y of the current point of the rod axis are calculated from formulae (5.4) and (5.5). In this way the deformed shape of the cantilever beam was obtained analytically.

As far as the numerical analysis of this problem is concerned, exactly the same geometrical and material data as those used in the previous example were adopted. Also the same finite element mesh was assumed.

The cantilever in various stages of deformations was shown in Fig. 7. The comparison between numerical and analytical solutions is presented in the Table 1.

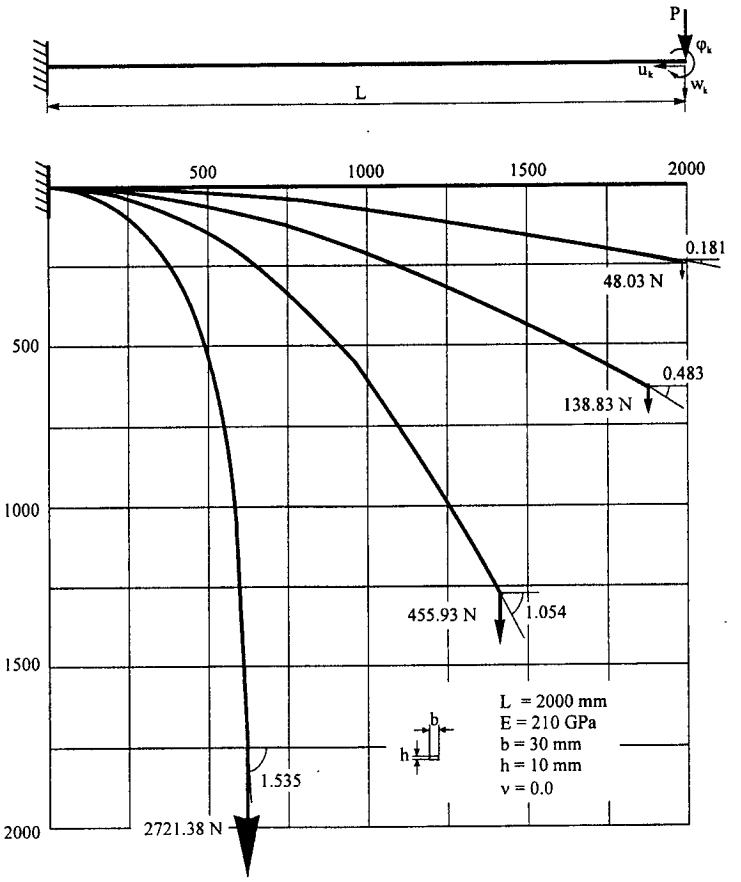

FIG. 7. Bending of the cantilever.

Table 1.

	Analytical solution			Numerical solution – relative error					
φ_k	w_k	u_k	P	w_k	error	u_k	error	P	error
[rad]	[mm]	[mm]	[N]	[mm]	%	[mm]	%	[N]	%
0.18055	240.03	17.369	47.967	240.00	0.01	17.37	0.01	48.03	0.12
0.48258	630.07	123.43	138.369	630.00	0.01	123.40	0.02	138.83	0.33
1.05408	1274.84	581.207	453.517	1275.00	0.01	581.25	0.01	455.93	0.53
1.53533	1741.24	1376.850	2702.240	1745.00	0.22	1380.42	0.26	2721.38	0.71

It is seen that the maximum relative error does not exceed 0.71%. It means that the coincidence of both solutions is nearly ideal.

5.3. Large deformations of the thin plate ring

The problem was presented by BUECHTER and RAMM [4]. It is a very severe test for programs taking into account finite rotations. The geometrical data of the ring and material properties are shown in Fig. 8a. The ring is cut along the segment AB. One side of this segment is completely fixed, the other is free and loaded by the vertical, uniformly distributed load of intensity $q = 100$ N/m.

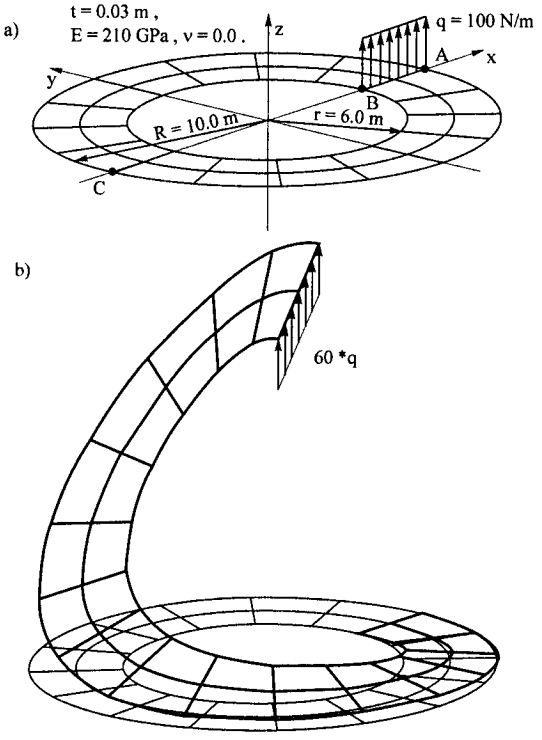

FIG. 8. Bending of the ring plate.

The finite element mesh is shown in Fig. 8a as well. The resulting discrete model has 365 d.o.f. The plate ring deforms due to the action of load increasing gradually. The deformed configuration for the load intensity $60q$ is shown in Fig. 8b. The maximum vertical displacements exceeds 15 m and the maximum angle of rotation reaches 1 rad.

Nonlinear equilibrium paths of three nodes of the plate ring are shown in Fig. 9. The obtained results were compared with those of BUECHTER and RAMM [4]. The correspondence of both solutions is satisfactory.

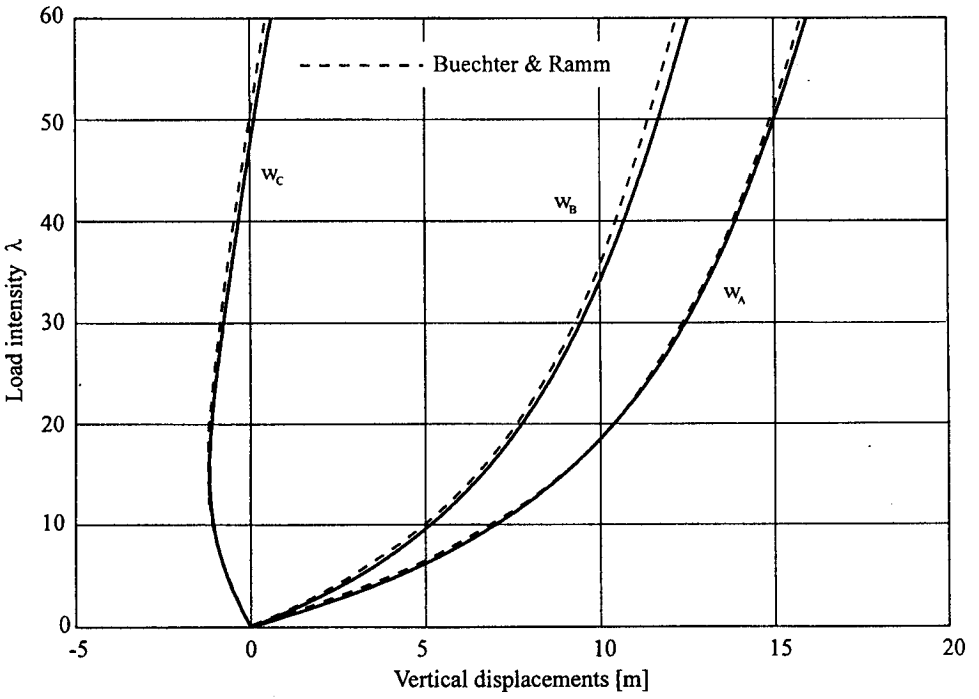

FIG. 9. Nonlinear equilibrium paths.

5.4. Large displacements and stability of the L-shaped plate strip

The L-shaped plate strip is shown in Fig. 10. The supporting manner and the whole geometry is shown in the same figure. The plate is of constant thickness $t = 0.6$ mm. Two cases of loading were considered. In the first case, load $F_x = \lambda P$ and was applied at the point C. In the second case $F_x = -\lambda P$ and was applied at the same point (cf. Fig. 10). Two finite element meshes were adopted. The first corresponds to the division into 15 elements (390 d.o.f.) and the other – into 60 elements (1225 d.o.f.). Both meshes are shown in Fig. 10.

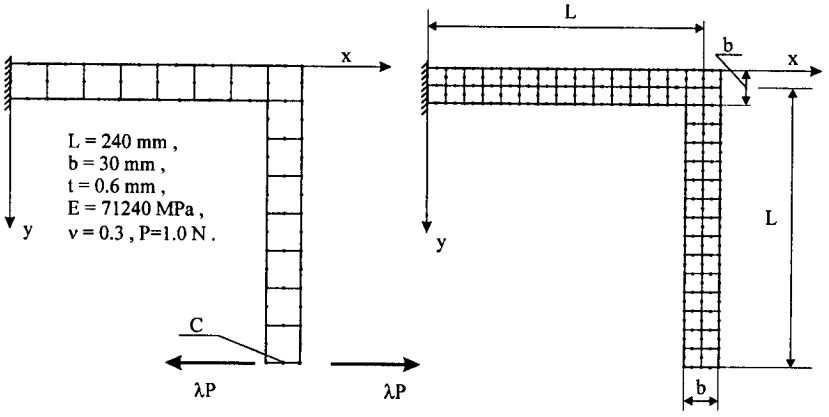

FIG. 10. L-shaped plate strip loaded by a concentrated force.

The analysis starts from the calculation of the fundamental paths. It has been found that the determinant of the tangent stiffness matrix changed its sign on the level $F_x = 1.2P$ in the first case of loading, and on the level $F_x = -0.71P$ in the second case of loading. It was the proof that the bifurcation paths existed on these levels of loads. Both bifurcation paths were determined by means of the load perturbation method, the details of which were presented elsewhere (cf. MARCINOWSKI [18]). As the perturbation load, the force $F_z = 0.001$ N was applied at the point C. This force was removed when the load-imperfection curve has reached the level $\lambda = 1.2$ or $\lambda = -0.7$ (the second case of loading). Fundamental and bifurcation paths are shown in Fig. 11 for both cases of loading and for both finite element meshes. Modes of deformations along bifurcation paths are shown as well. It is seen from paths $\lambda(u_c)$ that both bifurcation points are stable, symmetric points of bifurcation. Bifurcation paths are stable and it means that the plate strip has growing load carrying capacity in the postbuckling range.

Deformations in the postbuckling range are accompanied by large rotations. It is the reason that this problem can be solved only by means of programs which take into account finite rotations. Many authors have solved this problem and hence it is a good method of verification. The results of comparative analysis are presented in Fig. 12 in the form of bifurcation paths $\lambda(w_c)$ in a much wider range than it was shown in Fig. 11. Results of ARGYRIS *et al.* [19] and SIMO and VU-QUOC [20] refer to the beam model with large rotations and differ from the results of GRUTTMANN *et al.* [3], SIMO *et al.* [21] and CHRÓŚCIELEWSKI *et al.* [5], obtained by means of shell models with large rotations. Three different solutions were taken from the paper of CHRÓŚCIELEWSKI *et al.* [5]. They refer to two different kinds of finite elements. $e4$ denotes the quadrilateral four-node element whereas $e9$ means the quadrilateral nine-node element.

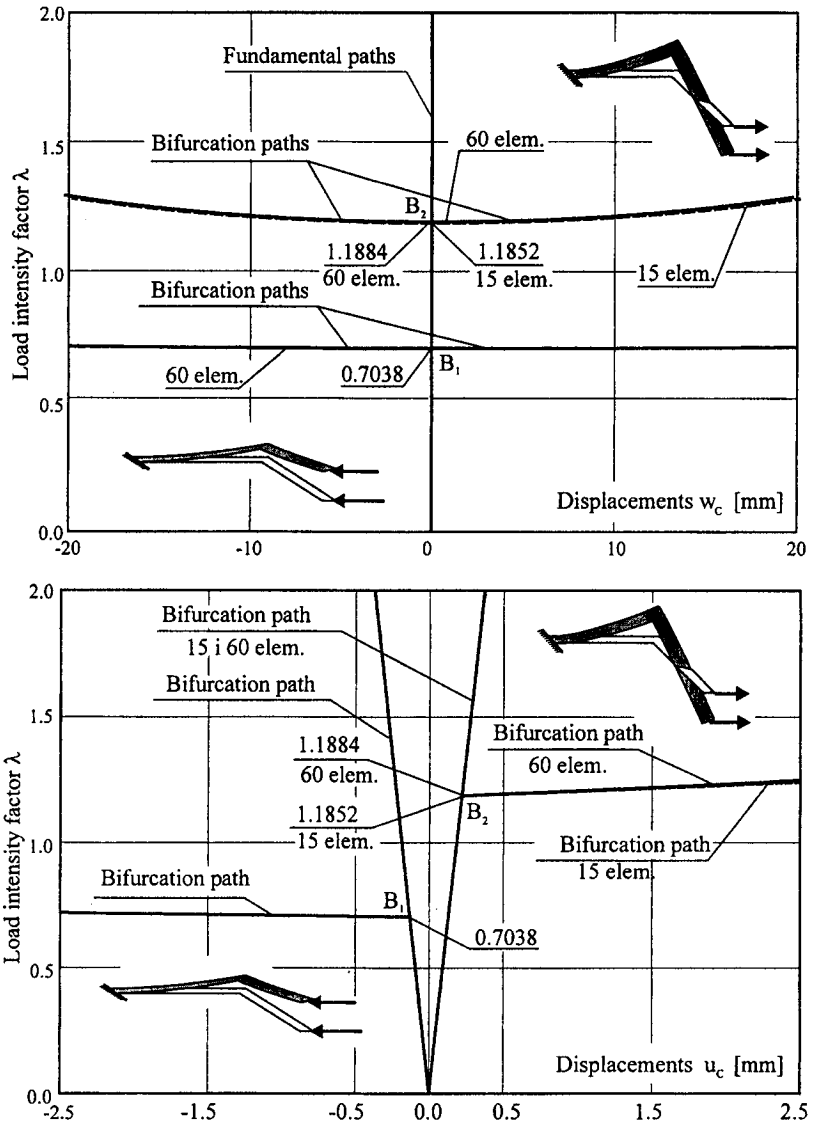

FIG. 11. Equilibrium paths $\lambda(w_c)$ and λu_c.

On the background of solutions of other authors, the present results were shown and these solutions are labelled 1 to 5. Curves 1, 2, 3 were obtained by means of a program which does not take into account large rotations. The curve 1 refers to the mesh of 15 elements whereas all other curves refer to the mesh of 60 elements. Curves 4 and 5 were obtained by means of the program in which the approach presented in the paper was implemented. Both refer to the mesh of 60 elements. Reference configurations were updated every time when the maximum

nodal rotation exceeded 0.05 rad in the initial range, and 0.02 rad in the final range of analysis.

The differences between the present solution (curve 4) and solutions of CHRÓŚCIELEWSKI seem to be very small. Unfortunately, none of the authors has presented the bifurcation path splitting at point B_1. There is no possibility of comparison of this solution. Small difference between solutions 2 and 5 can be explained by the absence of sufficiently large rotations (compare the mode of deformation in Fig. 12). The greatest one does not exceed 0.15 rad. In the first case of loading, the maximum rotation exceeded 0.75 rad and it is the source of such a considerable difference between solutions 3 and 4.

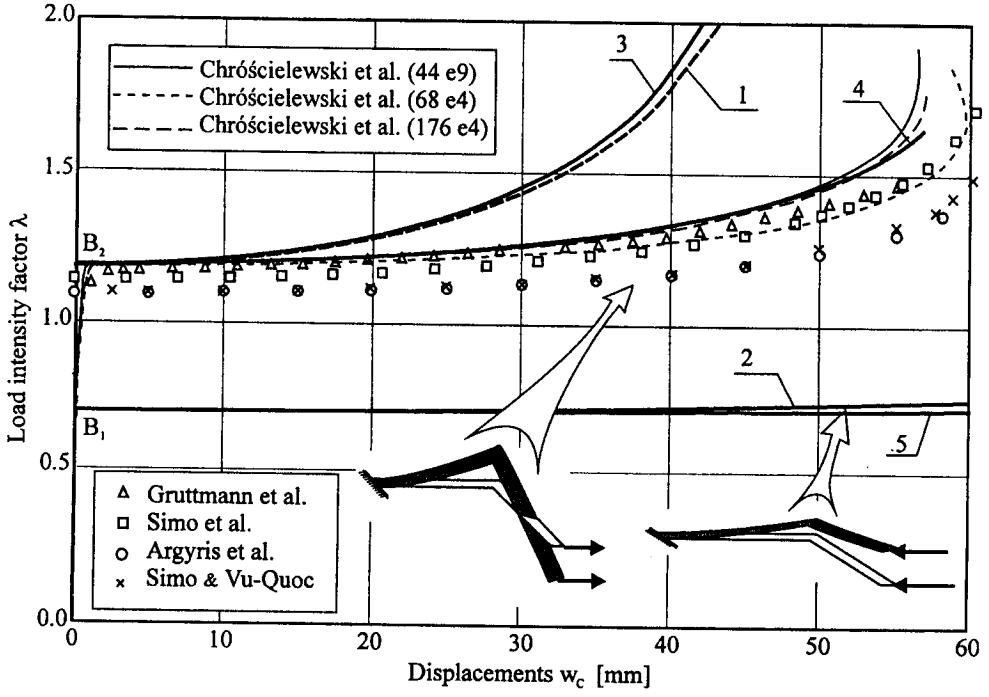

FIG. 12. A comparative analysis.

6. FINAL REMARKS

The idea of successive variation of the reference configuration presented in this paper in details, has made possible the description of deformations of shells with large rotations by means of the finite element formulation adequate essentially to problems with small or moderate rotations. It turned out that the degenerated finite element, being so effective in geometrically nonlinear problems

of shells with small or moderate rotations, can be used as well in geometrically nonlinear problems of shells with finite rotations. The governing equations of the problem were derived from the principle of virtual displacements written for the deformed configuration not free from stresses. This principle was reformulated into a discrete form according to the adopted degenerated finite element. Important problems related to the actualisation of reference configurations and to the calculation of stresses during the transition from the one reference configuration to the other were successfully solved. Details of the procedures used were presented. The idea of convected material coordinates turned out to be very effective in this case.

The presented examples have confirmed that the proposed approach is correct and can be applied to other problems concerning statics and stability of shells with large displacements and finite rotations.

REFERENCES

1. S. AHMAD, B. M. IRONS, O. C. ZIENKIEWICZ, *Analysis of thick and thin shell structures by curved finite elements*, Int. J. Num. Meth. Engng., **2**, 419–451, 1970.
2. J. MARCINOWSKI, *Calulation of nonlinear equilibrium paths of structures* [in Polish], Arch. of Civil Engng., **XXXV**, 3–4, 283–297, 1989.
3. F. GRUTTMANN, E. STEIN, P. WRIGGERS, *Theory and numerics of thin shells with finite rotations*, Ingenieur-Archiv, **59**, 54–67, 1989.
4. N. BUECHTER, E. RAMM, *Shell theory versus degeneration – a comparison in large rotation finite element analysis*, Int. J. Num. Meth. Engng., **34**, 39–59, 1992.
5. J. CHRÓŚCIELEWSKI, J. MAKOWSKI, H. STUMPF, *Genuinely resultant shell finite elements accounting for geometric and material nonlinearity*, Int. J. Num. Meth. Engng., **35**, 63–94, 1992.
6. C. SANSOUR, H. BUFLER, *An exact finite rotation shell theory, its mixed variational formulation and its finite element implementation*, Int. J. Num. Meth. Engng., **34**, 73–115, 1992.
7. K. S. SURANA, *Geometrically nonlinear formulation for the curved shell elements*, Int. J. Num. Meth. Engng., **19**, 581–615, 1983.
8. S. F. PAWSEY, R. W. CLOUGH, *Improved numerical integration of thick shell finite elements*, Int. J. Num. Meth. Engng., **3**, 575–586, 1971.
9. O. C. ZIENKIEWICZ, R. L. TAYLOR, J. M. TOO, *Reduced integration technique in general analysis of plates and shells*, Int. J. Num. Meth. Engng., **3**, 275–290, 1971.
10. K. J. BATHE, E. RAMM, E. L. WILSON, *Finite element formulation for large deformation dynamic analysis*, Int. J. Num. Meth. Engng., **9**, 353–386, 1975.
11. J. A. STRICKLIN, W. E. HAISLER, *Formulations and solution procedures for nonlinear structural analysis*, Computers and Structures, **7**, 123–136, 1977.

12. L. E. MALVERN, *Introduction to the mechanics of a continuous medium*, Prentice-Hall, Inc., Englewood Cliffs, New Jersey 1969.

13. O. C. ZIENKIEWICZ, *Finite element method* [in Polish], Arkady, Warszawa 1972.

14. J. MARCINOWSKI, D. ANTONIAK, *Stability of the cylindrical panel. Experimental investigations and numerical analysis*, Engng. Trans., **42**, 1–2, 61–74, 1994.

15. J. T. ODEN, *Finite elements of nonlinear continua*, McGraw-Hill, Inc., 1972.

16. M. KLEIBER, *Finite element method in nonlinear mechanics of solids* [in Polish], PWN, Warszawa-Poznań 1985.

17. R. FRISCH-FAY, *A new approach to the analysis of the deflection of thin cantilevers*, Proc. ASCE, J. Appl. Mech., **28**, 87–90, 1961.

18. J. MARCINOWSKI, *Bifurcation points and branching paths in the nonlinear stability analysis of shell structures*, J. Theoret. Appl. Mech., **32**, 3, 637–651, 1994.

19. J. H. ARGYRIS, H. BALMER, J. ST. DOLTSINIS, P. C. DUNNE, M. HAASE, M. KLEIBER, G. MALEJANNAKIS, H. P. MLEJNEK, M. MÜLLER, D. W. SCHARPF, *Finite element method – natural approach*, Comp. Meth. Appl. Mech. Engng., **17/18**, 1–106, 1979.

20. J. C. SIMO, L. VU-QUOC, *Three-dimensional finite-strain rod model. Part II Computational aspects*, Comp. Meth. Appl. Mech. Engng., **58**, 79–116, 1986.

21. J. C. SIMO, D. D. FOX, M. S. RIFAI, *On a stress resultant geometrically exact shell model. Part III: Computational aspects of the nonlinear theory*, Comp. Meth. Appl. Mech. Engng., **79**, 21–70, 1990.

Received October 22, 1999; revised version March 29, 2000.